



HAL
open science

Development of a Novel Hydrophobic ZrO₂–SiO₂ Based Acid Catalyst for Catalytic Esterification of Glycerol with Oleic Acid

Pei San Kong, Patrick Cognet, Yolande Peres-Lucchese, Jérôme Esvan, Wan Mohd Ashri Wan Daud, Mohamed Kheireddine Aroua

► **To cite this version:**

Pei San Kong, Patrick Cognet, Yolande Peres-Lucchese, Jérôme Esvan, Wan Mohd Ashri Wan Daud, et al.. Development of a Novel Hydrophobic ZrO₂–SiO₂ Based Acid Catalyst for Catalytic Esterification of Glycerol with Oleic Acid. *Industrial and engineering chemistry research*, 2018, 57 (29), pp.9386-9399. 10.1021/acs.iecr.8b01609 . hal-01951473

HAL Id: hal-01951473

<https://hal.science/hal-01951473>

Submitted on 11 Dec 2018

HAL is a multi-disciplinary open access archive for the deposit and dissemination of scientific research documents, whether they are published or not. The documents may come from teaching and research institutions in France or abroad, or from public or private research centers.

L'archive ouverte pluridisciplinaire **HAL**, est destinée au dépôt et à la diffusion de documents scientifiques de niveau recherche, publiés ou non, émanant des établissements d'enseignement et de recherche français ou étrangers, des laboratoires publics ou privés.



Open Archive Toulouse Archive Ouverte (OATAO)

OATAO is an open access repository that collects the work of Toulouse researchers and makes it freely available over the web where possible

This is an author's version published in: <http://oatao.univ-toulouse.fr/21093>

Official URL: <https://doi.org/10.1021/acs.iecr.8b01609>

To cite this version:

Kong, Pei San[✉] and Cagnet, Patrick[✉] and Peres-Lucchese, Yolande[✉] and Esvan, Jérôme[✉] and Daud, Wan Mohd Ashri Wan and Aroua, Mohamed Kheireddine *Development of a Novel Hydrophobic ZrO₂-SiO₂ Based Acid Catalyst for Catalytic Esterification of Glycerol with Oleic Acid.* (2018) *Industrial & Engineering Chemistry Research*, 57 (29). 9386-9399. ISSN 0888-5885

Any correspondence concerning this service should be sent to the repository administrator: tech-oatao@listes-diff.inp-toulouse.fr

Development of a Novel Hydrophobic ZrO₂–SiO₂ Based Acid Catalyst for Catalytic Esterification of Glycerol with Oleic Acid

Pei San Kong,^{†,§} Patrick Cognet,[†] Yolande Pérès,[†] Jerome Esvan,[‡] Wan Mohd Ashri Wan Daud,[§] and Mohamed Kheireddine Aroua^{*,||,⊥}

[†]Laboratoire de Génie Chimique (Labège), BP 84234 Campus INP ENSIACET, 4 allée Emile Monso, 31432 Toulouse Cedex 4, France

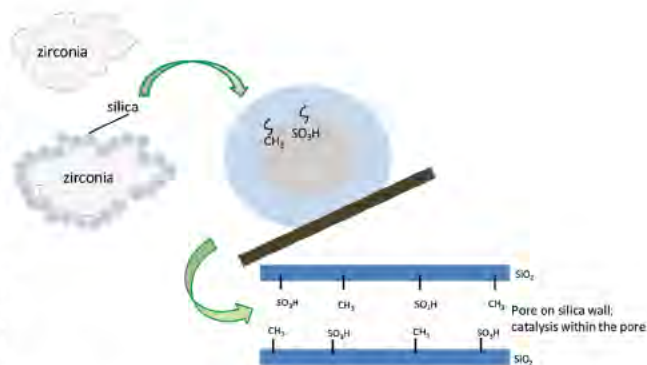
[‡]CIRIMAT (Labège), BP 84234 Campus INP ENSIACET, 4 allée Emile Monso, 31432 Toulouse Cedex 4, France

[§]Department of Chemical Engineering, Faculty of Engineering, University of Malaya, 50603 Kuala Lumpur, Malaysia

^{||}Centre for Carbon Dioxide Capture and Utilization (CCDCU), School of Science and Technology, Sunway University, Bandar Sunway, 47500 Petaling Jaya, Malaysia

[⊥]Department of Engineering, Lancaster University, Lancaster, LA1 4YW, United Kingdom

ABSTRACT: The inevitably low value of glycerol has led to extensive investigations on glycerol conversion to value added derivatives. The esterification of glycerol with oleic acid is currently a very important industrial process. In this work, a novel heterogeneous acid catalyst featuring hydrophobic surface is developed on modified ZrO₂–SiO₂ support as water tolerant solid acid catalyst is vital for biphasic esterification reactions that produce water. The novel ZrO₂–SiO₂–Me&Et PhSO₃H catalyst was prepared through silication and surface modification with trimethoxymethylsilane and 2 (4 chlorosulfonylphenyl)ethyltrimethoxysilane. This work showed that it is possible to control the acidity and hydrophobicity of the catalyst by tailoring the amount of surface modification agents. It was found that the hydrophobicity of the catalyst decreased as its acidity increased. Furthermore, at constant catalyst acidity, the more hydrophobic catalyst showed a better yield.



1. INTRODUCTION

Glycerol is the byproduct primarily produced from oleochemicals and the biodiesel industry. Intensive research has been focused in transforming glycerol into higher value added derivatives due to the drastic surplus of glycerol in the chemical market.¹ In mid 2017, the reported crude glycerol and refined glycerol prices were \$0.24/kg and \$0.8/kg, respectively.² Heterogeneous acid catalysts are widely used in the conversion of glycerol into valuable derivatives such as dehydration to acrolein, acetylation to triacetin, esterification to glycerol esters, etherification to polyglycerols or glycerol ether, and condensation to 1,3 dioxolanes and 1,3 dioxanes.^{3–5} One promising option is the catalytic esterification of glycerol to obtain mono and diesters. Typically, the esterification reaction of glycerol with oleic acid (OA; a common unsaturated fatty acid with C18:1 carbon chain) is a feasible and economical method to change the fatty acid profile of a triglyceride. A mixture of glycerol monooleate (GMO), glycerol dioleate (GDO), and glycerol trioleate (GTO) can be produced over acid catalyzed esterification reaction, according to the reaction scheme in Figure 1.

The esterification of glycerol with OA is important and has been investigated extensively due to its high commercial value and numerous applications.^{6–8} GMO and GDO are lipids with amphiphilic, nonionic, and excellent emulsifying properties as they contain a hydrophilic head and a hydrophobic tail that result in surfactant/emulsifier properties.⁹ Both GMO and GDO are extensively employed in the food, cosmetic, and pharmaceutical industries, whereby GDO is known as a safe plasticizer for the polymer industry. GTO is mainly applied as a biolubricant in food and medical machinery and is produced via conventional acid catalyzed esterification of glycerol with OA. Currently, there are three major routes to produce GMO and GDO: (i) base catalyzed glycerolysis of triolein with glycerol at elevated temperature of 250 °C; (ii) alkali glycerolysis of methyl oleate at high reaction temperature; (iii) enzymatic/acid catalyzed esterification of glycerol with OA.¹⁰

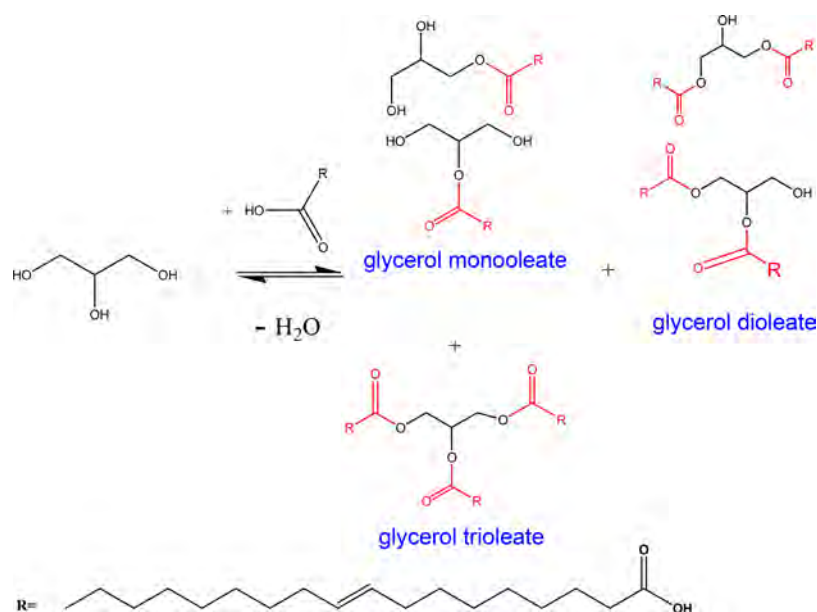


Figure 1. Reaction scheme for esterification of glycerol with OA.

The heterogeneous acid catalyzed esterification route is known to be more selective and cost effective compared to the aforementioned routes.⁶ In addition, the heterogeneous acid catalytic system is environmentally sustainable compared to homogeneous catalyst, due to less waste production, easier operation, and possible recycling. However, the catalytic activity of a heterogeneous catalyst is generally lower than that of a homogeneous one due to the poor accessibility of the embedded catalytic sites. The highly desirable selectivity of the product can be obtained using a heterogeneous catalyst system, as the textural property of catalyst, such as porosity, might influence product selectivity.^{11,12} In fact, the use of glycerol as a starting material to produce glycerol derivatives is challenging. The high viscosity of glycerol could encounter a diffusion problem in reaction media. Moreover, it has been reported that the reaction, involving reactants in two different phases, is complicated; for instance, poor interaction of OA and glycerol leads to low reactivity in the esterification process¹³ as well as reaction of glycerol with poorly soluble acetone in the acetalization production of solketal.^{14,15} Some of the researchers elucidate that hydrophobicity enhanced acid catalysts can improve reactivity as well as selectivity, especially when one of the reactants is highly hydrophilic.^{7,16,17} Moreover, the presence of water byproduct in a typical esterification reaction can easily deactivate the acid sites of solid acid catalyst and negatively affect the equilibrium of reaction.¹⁸ Consequently, water tolerant solid acid catalyst featuring a hydrophobic surface is vital for the esterification of glycerol with fatty acid.¹⁹

Ion exchange resins,²⁰ zeolites,⁶ double metal cyanide complexes,²¹ heteropolyacid supported catalysts,²² hydrotalcite,^{23,24} and metal oxide based acid catalysts¹⁰ have been studied for catalytic glycerol esterification with OA. It was reported that Sn- β zeolite catalyzed esterification was inefficient with only 4% OA conversion after 20 h reaction at equimolar ratio, 150 °C, and solvent added condition, even below the conversion without adding any catalyst (20%) at identical reaction parameters.²² By contrast, hydrophobicity enhanced catalysts such as titanasilicate catalyst²⁵ and ionic liquid grafted catalyst²⁶ were investigated and reportedly can

promote interaction of reactants and higher GMO selectivity can be achieved.

Therefore, this study aims to design a highly hydrophobic functional heterogeneous acid catalyst for catalytic esterification of glycerol with OA at mild reaction condition. It was reported that mesoporous polystyrene sulfonic acid and inorganic oxide composites are favorable due to their tunable surface wettability (hydrophobicity and hydrophilicity), engineered textural properties, and acidity.¹⁹ Development of an organosulfonic acid functionalized on silica coated zirconia (ZrO₂-SiO₂) is proposed in this work. To the best of our knowledge, development of such a hydrophobic ZrO₂-SiO₂ based acid catalyst has not been reported in the available literature. The intention to select zirconia (ZrO₂) as the catalyst's support is due to its highly attractive support material among various metal oxides. ZrO₂ generally has low surface area but moderate surface acidity. By contrast, silica (SiO₂) has higher surface area but lower surface acidity. As such, coating of SiO₂ on ZrO₂ eventually can increase the surface area, stability, and acidity of the ZrO₂-SiO₂ system compared to individual ZrO₂ or SiO₂. It has been reported that Si doping stabilizes the tetragonal ZrO₂ phase.^{11,27} A recent study on iron oxide supported SiO₂ catalyst has successfully created covalent Si-O bonds that minimize leaching of the ligand moiety of the catalyst.²⁸ Therefore, development of hydrophobic silica supported sulfonic acid type catalysts is expected favoring a better diffusion within the pore framework and enabling shape selectivity effect.

In this work, the preparation and characterization of highly hydrophobic organosulfonic acid functionalized ZrO₂-SiO₂ catalyst is investigated. Each catalyst modification step, from the preparation of ZrO₂ to functionalization, has been carefully studied, and the obtained structures have been confirmed with characterization results. Moreover, an original technique to control acidity and the hydrophobicity level of the designed catalyst is disclosed. The role of the hydrophobicity of the designed catalyst is studied herein by comparing the reaction rate and yield of GMO in esterification of glycerol with OA. The objective is to maximize the GMO yield; therefore, an equimolar ratio of reactants was employed. In addition, the

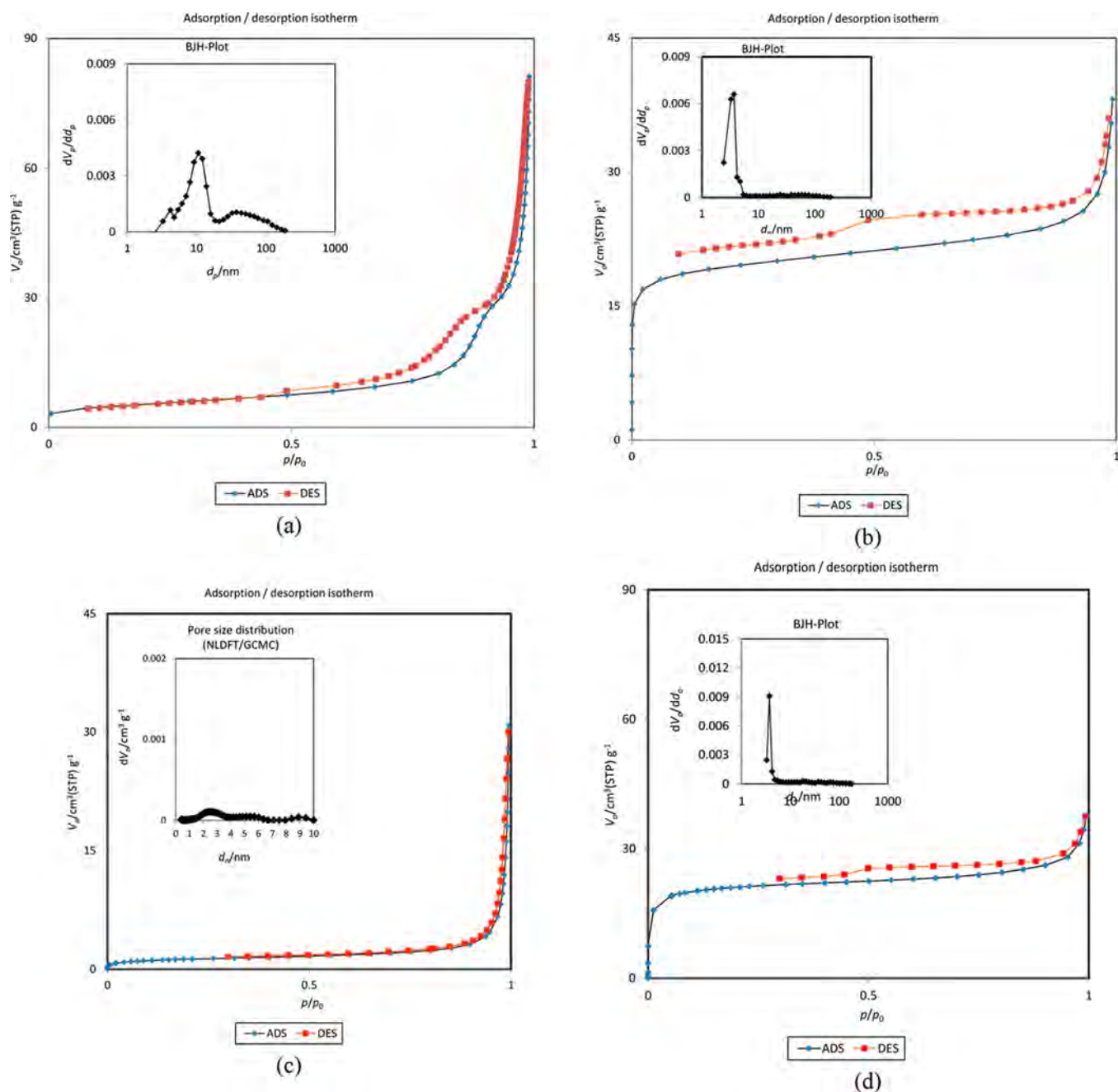


Figure 2. N_2 adsorption–desorption isotherms and BJH plots for ZrO_2 (a), ZrO_2-SiO_2 (b), $ZrO_2-SiO_2-Me\&Et\ PhSO_2Cl$ (c), and $ZrO_2-SiO_2-Me\&Et\ PhSO_3H$ (d).

surface mechanism of the catalyst modification is proposed according to comprehensive characterization and catalytic activity results.

2. EXPERIMENTAL SECTION

2.1. Materials. Zirconia (97%), ethanol (99%), ammonia solution (25 wt %), tetraethyl orthosilicate (TEOS, 98%), trimethoxymethylsilane (TMMS, 98%), dry toluene (99%), and sulfuric acid (99.99%) were purchased from Sigma Aldrich. 2-(4-Chlorosulfonylphenyl)ethyltrimethoxysilane (CSPETS, 50% in dichloromethane) was purchased from Fisher Scientific. Reactants glycerol ($\geq 99.5\%$) and OA (technical grade, 90%) were purchased from Sigma Aldrich. These reagents were used without purification unless otherwise

stated. All the analytical standard reagents such as GMO ($\geq 99\%$), GDO ($\geq 99\%$), and GTO ($\geq 99\%$) were purchased from Sigma Aldrich. Analytical grade solvents such as acetonitrile (ACN), methanol (MeOH), and tetrahydrofuran (THF) were used as mobile phase for quantification analysis. Trifluoroacetic acid (TFA) was used as mobile phase additive due to its high resolving power.

2.2. Catalyst Preparation. The coating of SiO_2 on ZrO_2 was synthesized using hydrolysis and co condensation method. A 2 g sample of ZrO_2 was added into 100 mL of ethanol under vigorous mixing at ambient temperature for 30 min. A 12 mL volume of 25% ammonia solution (NH_4OH) and 4 mL of TEOS were successively added into the mixture. The resulted solution was continuously stirred and aged for 24 h. The

resulted powder (ZrO₂-SiO₂) was then filtered, rinsed with ethanol, and dried under vacuum at room temperature. Turning of ZrO₂-SiO₂ into higher hydrophobicity level and functionalization of sulfonic acid group on the support was performed using TMMS and CSPETS, respectively.²⁹ Varied amounts of CSPETS and TMMS were added into a 35 mL of dry toluene that contained 1 g of SiO₂-ZrO₂ and was continuously stirred for 24 h. Subsequently, the functionalized catalyst (ZrO₂-SiO₂-Me&Et PhSO₂Cl) was washed with toluene (2 × 15 mL) and distilled water. Lastly, the modified solids were suspended in H₂SO₄ aqueous solution for 2 h. The final catalyst (ZrO₂-SiO₂-Me&Et PhSO₃H) was washed with water and dried overnight under vacuum at room temperature.

2.3. Catalyst Characterizations. The textural properties of the catalysts were measured by N₂ adsorption-desorption using a BELSORP max analyzer (Japan). The solid catalysts were outgassed by vacuum at 200 °C for 5 h. The particle size distributions of samples were measured by a Malvern MS3000 particle sizer at 2 bar. The morphology of the surface catalyst was captured by a field emission scanning electron microscope (FESEM) at 1–30 kV acceleration voltage using model JSM 7100F. The hydrophobicity level of the catalyst was measured by the water contact angle method using a KRUSS DSA100 instrument. The catalyst was pressed into a pellet at 8 MPa prior to analysis. The acidity of the catalyst was determined by acid-base titration with 8.38 × 10⁻³ M NaOH solution.¹⁹ A 40–50 mg sample of catalyst was degassed at 120 °C for 3 h and then stirred in 25 mL of NaCl (2 M) for 24 h at room temperature. The resulting suspension was titrated with NaOH solution. Thermogravimetric analysis (TGA) technique was performed to ascertain the thermal stability of catalysts using a Mettler Toledo system at a rate of 10 °C/min from 25 °C to a maximum temperature of 900 °C. Meanwhile, Fourier transform infrared (FT IR) spectra were obtained using a Bruker IR spectrometer in the range 200–4000 cm⁻¹. X ray photoelectron spectra (XPS) were performed using a ThermoScientific Kalpha device. The samples were analyzed at a pressure of approximately 5 × 10⁻⁹ Pa recorded by Al Kα radiation.

2.4. Catalytic Reaction and Analysis. The catalytic esterification of glycerol with OA was performed in a batch reactor connected to a condenser and a vacuum system at 100 °C for 8 h using three catalysts designed with different hydrophilicities: ZrO₂-SiO₂-Me&Et PhSO₃H 50, ZrO₂-SiO₂-Me&Et PhSO₃H 70, and ZrO₂-SiO₂-Me&Et PhSO₃H 80 (values of 80, 70, and 50 at the ends of the catalyst symbols indicate the mole percentage of TMMS utilized in tailoring the hydrophobicity level of the catalysts). The products were analyzed by high performance liquid chromatography with refractive index detection (HPLC RI) and a Gemini C18 110A column (100 mm × 2 mm × 3 μm). Isocratic method was used in separation and quantitative determination. The OA and GMO groups of the sample were separated using a mobile phase consisting of ACN/water (80:20 v/v) with 0.1% TFA (v/v of total mobile phase); GDO and GTO groups were separated using ACN/MeOH/THF (40:40:20 v/v/v).³⁰ The injection volume was 10 μL, and the diluted samples were eluted at a 220 μL/min flow rate. The column and RI detector temperatures were set at 40 °C. The conversion, yield, and selectivity of the products were calculated according to eq 1, 2, and 3, respectively.

$$\text{conversion} = \frac{\text{mol}_{\text{OA consumed}}}{\text{mol}_{\text{OA initial}}} \times 100\% \quad (1)$$

$$\text{yield}_{\text{total GMO,GDO,GTO}} = \frac{\text{mol}_{\text{total esters}}}{\text{mol}_{\text{OA initial}}} \times 100\% \quad (2)$$

$$\text{selectivity}_{\text{GMO}} = \frac{\text{mol}_{\text{GMO}}}{\text{mol}_{\text{total GMO+GDO+GTO}}} \times 100\% \quad (3)$$

3. RESULTS AND DISCUSSION

3.1. Catalyst Characterizations. **3.1.1. Physicochemical and Textural Properties of Catalysts.** **3.1.1.1. Pore Size Distribution.** N₂ physisorption was utilized to measure the surface area, pore size distribution, and porosity of the catalysts. Figure 2a shows the N₂ adsorption-desorption isotherm plots for ZrO₂ support. ZrO₂ showed a superposition of type IV isotherm with hysteresis loop at a relative pressure range of 0.5–1.0. This result indicated that the pore size distributions are given by nonrigid aggregates of plate like particles and mainly composed of mesopores and a minority of macropores.³¹ Results also confirmed that the ZrO₂ used in this study possessed meso-macropore pore sizes, with pore size ranging from 10.57 to 120 nm. The sintering process occurred at high calcination temperature, which resulted in the removal of OH⁻ from ZrO₂ and formation of large pore size for ZrO₂. The obtained result is similar to that reported in Zhao et al.³²; those authors indicated that the surface area of a solid material decreases, and its average pore diameter increases, with increased calcination temperature.

Figure 2b displays a sharp increase in the loading of the ZrO₂-SiO₂ catalyst at low values of p/p_0 , which suggested a high surface area support. The presence of hysteresis type IV isotherm in this plot showed that the obtained pore size distribution was consistent, with small pore size within the mesoporous range. SiO₂ was mainly adsorbed on the inner wall and fitted inside the ZrO₂ support, which significantly reduced the average pore diameter of ZrO₂-SiO₂ from 120 to 3.71 nm. Therefore, the SiO₂ active species were well deposited on the support, which was evidenced by its pore size distribution curve. The increased surface area of ZrO₂-SiO₂ can be explained by the adherence of new SiO₂ phase on the ZrO₂ support, which led to the formation of rough, heterogeneous, and well deposited small particles on the catalyst support.

The N₂ adsorption isotherm of the catalyst functionalized with TMMS and CSPETS, that is, ZrO₂-SiO₂-Me&Et PhSO₂Cl, is presented in Figure 2c. The obtained hysteresis plot of the ZrO₂-SiO₂-Me&Et PhSO₂Cl catalyst indicated a low porosity adsorbent because the adsorbent-adsorbate interactions were relatively weak. Unlike the ZrO₂ support or ZrO₂-SiO₂, the average pore diameter for the ZrO₂-SiO₂-Me&Et PhSO₂Cl catalyst was determined using the non localized density functional theory (NLDFT)/grand canonical Monte Carlo (GCMC) method due to its incompatibility with the Barrett-Joyner-Halenda (BJH) model. Notably, the average pore diameter of the prepared catalyst in the third step (ZrO₂-SiO₂-Me&Et PhSO₂Cl, 2.24 nm) was slightly smaller than that of ZrO₂-SiO₂ (3.77 nm), which suggested the grafting of agents on the surface of ZrO₂-SiO₂. The TMMS-CSPETS hypothesis was proposed, and the functionalized ZrO₂-SiO₂ support was proven in this characterization analysis.

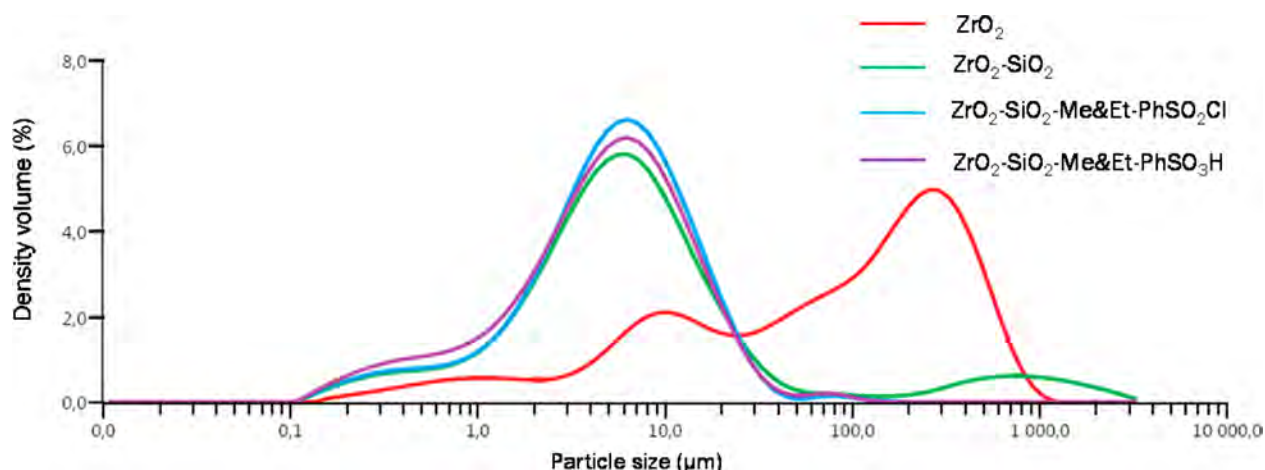


Figure 3. Particle size distribution curves for ZrO_2 , $\text{ZrO}_2\text{-SiO}_2$, $\text{ZrO}_2\text{-SiO}_2\text{-Me\&Et-PhSO}_2\text{Cl}$, and $\text{ZrO}_2\text{-SiO}_2\text{-Me\&Et-PhSO}_3\text{H}$.

Table 1. Physicochemical Properties of Functionalized Catalysts in Each Modification Step

catalyst	area ^a (m ² /g)	pore vol ^b (cm ³ /g)	av pore diam ^b (nm)	av particle diam ^c (μm)	acidity (mmol/g)
ZrO_2	18.77	0.13	10.70	100.00	0.18
$\text{SiO}_2\text{-ZrO}_2$	73.05	0.030	3.77	5.87	0.00
$\text{ZrO}_2\text{-SiO}_2\text{-Me\&Et-PhSO}_2\text{Cl}^d$		0.032	2.24	5.39	0.16
$\text{ZrO}_2\text{-SiO}_2\text{-Me\&Et-PhSO}_3\text{H}$	79.75	0.025	3.77	5.01	0.62

^aTotal surface area was determined using BET equation. ^bPore volume and average pore diameter were determined using BJH method. ^cParticle diameter was measured by Mastersizer. ^dPore volume and average pore diameter were determined using NLDFT/GCMC method.

The acidification of functionalized catalyst ($\text{ZrO}_2\text{-SiO}_2\text{-Me\&Et-PhSO}_3\text{H}$) exhibited a hysteresis loop at a relative pressure range of 0.3–0.8, as shown in Figure 2d. The hysteresis loop of the $\text{ZrO}_2\text{-SiO}_2\text{-Me\&Et-PhSO}_3\text{H}$ catalyst ranged between those of $\text{ZrO}_2\text{-SiO}_2\text{-Me\&Et-PhSO}_2\text{Cl}$ and $\text{ZrO}_2\text{-SiO}_2$. This result indicated that sulfonation removed some of the agents of $\text{ZrO}_2\text{-SiO}_2\text{-Me\&Et-PhSO}_2\text{Cl}$. Comparison of the hysteresis curve and pore diameter plot of $\text{ZrO}_2\text{-SiO}_2\text{-Me\&Et-PhSO}_3\text{H}$ to $\text{ZrO}_2\text{-SiO}_2$ hysteresis loop (Figure 2b) confirmed that $\text{ZrO}_2\text{-SiO}_2\text{-Me\&Et-PhSO}_3\text{H}$ is a mesoporous catalyst.

3.1.1.2. Particle Size Distribution. The particle size distribution curves of the catalysts prepared at four different modification steps are shown in Figure 3. Results revealed that coating the ZrO_2 support with SiO_2 altered the particle size distribution range from a broad wide range to a narrow range and bell shaped distribution. This result may be attributed to the incorporation of Si atom into the Zr support. Nevertheless, this work indicated that functionalization of hydrophobic agent and sulfonation process exerted no effect on the particle size distribution of the catalysts. Moreover, the particle size distributions of $\text{ZrO}_2\text{-SiO}_2$, $\text{ZrO}_2\text{-SiO}_2\text{-Me\&Et-PhSO}_2\text{Cl}$, and $\text{ZrO}_2\text{-SiO}_2\text{-Me\&Et-PhSO}_3\text{H}$ were identical.

3.1.1.3. Acidity. The catalyst acidity at four different modification steps was measured. Table 1 summarizes the physicochemical and textural properties of the functionalized catalyst in each modification step. The original ZrO_2 showed low acidity value (0.18 mmol/g) because ZrO_2 is naturally a Brønsted base. Notably, the silication step reduced the ZrO_2 acidity from 0.18 to 0.00 mmol/g. This effect can be explained by the fact that the NH_4OH used to catalyze the hydrolysis and condensation reaction in the silication step changed the surface acidity of the original ZrO_2 due to neutralization and silica coating. The zero acidity of $\text{SiO}_2\text{-ZrO}_2$ indicates that SiO_2 was well coated on the ZrO_2 support. The acidity of the

third step prepared $\text{SiO}_2\text{-Me\&Et-PhSO}_2\text{Cl}$ catalyst was 0.16 mmol/g. The acidity of the $\text{ZrO}_2\text{-SiO}_2\text{-Me\&Et-PhSO}_3\text{H}$ catalyst was increased to 0.62 mmol/g after the acidification step.

3.1.2. Morphology Characterization. Images of the different development stages of the catalyst were captured by using high resolution FESEM and are displayed in Figure 4. ZrO_2

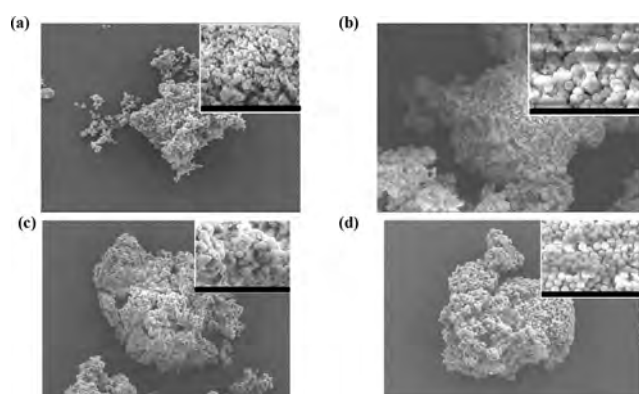


Figure 4. FESEM morphologies of ZrO_2 (a), $\text{ZrO}_2\text{-SiO}_2$ (b), $\text{ZrO}_2\text{-SiO}_2\text{-Me\&Et-PhSO}_2\text{Cl}$ (c), and $\text{ZrO}_2\text{-SiO}_2\text{-Me\&Et-PhSO}_3\text{H}$ (d).

presented typical rough, meso–macropore space and irregular surface morphology (Figure 4a). The uneven ZrO_2 surface can be associated with material sintering during drying and calcination processes. Nevertheless, the presence of silica like substance on ZrO_2 support was supported by the latter modified $\text{ZrO}_2\text{-SiO}_2$ (Figure 4b). The hydrolysis and condensation processes used in the silica coating of this work were according to the modified Stöber method. The base catalyzed hydrolysis and successive condensation of TEOS result in the formation of monodispersed spherical

silica particle.³³ The spherical shape particles evolve when the chemical bond and van der Waals forces generate elastic and plastic deformations between two oligomers; eventually, two oligomers engulf each other to maintain the spherical shape.³⁴

The addition of both TMMS and CSPETS agents resulted in no modification on the surface morphology of $\text{ZrO}_2\text{-SiO}_2\text{-Me\&Et PhSO}_2\text{Cl}$. However, smearing of the silica like substance was observed (Figure 4c). $\text{ZrO}_2\text{-SiO}_2\text{-Me\&Et PhSO}_3\text{H}$ catalyst (Figure 4d) significantly displayed uniform and smooth spherical particles with consistent sizes. The pore diameter of a single silica sphere was approximately 400 nm. The overnight aging in the silication process and using excessive ethanol in washing of $\text{ZrO}_2\text{-SiO}_2$ has produced porosity type particles because the hydrolysis of alkoxy groups and condensation and re esterification of silanol groups upon reimmersion in ethanol result in the formation of micro-mesoporous silica.³⁵ Thus, the morphology images are correlated with the aforementioned Brunauer–Emmett–Teller (BET) results.

3.1.3. Thermogravimetric Analysis (TGA). The TGA curves of ZrO_2 , $\text{ZrO}_2\text{-SiO}_2$, $\text{ZrO}_2\text{-SiO}_2\text{-Me\&Et PhSO}_2\text{Cl}$, and $\text{ZrO}_2\text{-SiO}_2\text{-Me\&Et PhSO}_3\text{H}$ are shown in Figure 5. A weight

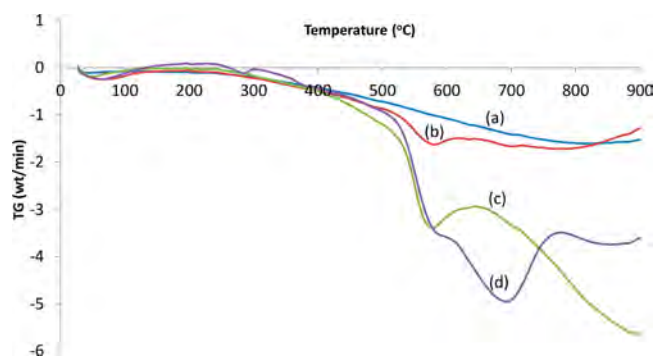


Figure 5. TGA curves for ZrO_2 (a), $\text{ZrO}_2\text{-SiO}_2$ (b), $\text{ZrO}_2\text{-SiO}_2\text{-Me\&Et PhSO}_2\text{Cl}$ (c), and $\text{ZrO}_2\text{-SiO}_2\text{-Me\&Et PhSO}_3\text{H}$ (d) on the basis of the weight loss rate.

loss occurred in the $\text{ZrO}_2\text{-SiO}_2\text{-Me\&Et PhSO}_3\text{H}$ catalyst at a temperature range of 260–300 °C. This weight loss was 4 wt % in $\text{ZrO}_2\text{-SiO}_2\text{-Me\&Et PhSO}_3\text{H}$ compared with the third

step prepared $\text{ZrO}_2\text{-SiO}_2\text{-Me\&Et PhSO}_2\text{Cl}$, which indicated the decomposition of the sulfate moiety.³⁶ The second weight loss zone was observed at 560–570 °C for $\text{ZrO}_2\text{-SiO}_2$, $\text{ZrO}_2\text{-SiO}_2\text{-Me\&Et PhSO}_2\text{Cl}$, and $\text{ZrO}_2\text{-SiO}_2\text{-Me\&Et PhSO}_3\text{H}$; this loss was attributed to the decomposition of SiO_2 material.¹⁷ These weight losses were significant, especially for functionalized $\text{ZrO}_2\text{-SiO}_2\text{-Me\&Et PhSO}_2\text{Cl}$ and $\text{ZrO}_2\text{-SiO}_2\text{-Me\&Et PhSO}_3\text{H}$. TGA analysis showed that ZrO_2 support possessed good thermal stability. Therefore, the catalytic reaction is within the thermal stability range of catalyst for the reaction temperature of approximately 250 °C.

3.1.4. Hydrophobicity. The hydrophobicity of the developed catalyst should be measured when developing highly hydrophobic and heterogeneous acid catalyst. The hydrophobicity level of each developed catalyst was determined by contact angle analysis, and results are presented in Figure 6. The water contact angle of the catalyst was increased in the order $\text{ZrO}_2\text{-SiO}_2\text{-Me\&Et PhSO}_3\text{H} > \text{ZrO}_2\text{-SiO}_2\text{-Me\&Et PhSO}_2\text{Cl} > \text{ZrO}_2\text{-SiO}_2 > \text{ZrO}_2$. Noticeably, the lowest hydrophobicity was shown by the original ZrO_2 support. Hydrophobicity was enhanced through coating ZrO_2 support with SiO_2 ; this effect was attributed to that the siliceous material improved the hydrophobic environment because Si atom can increase the hydrophobicity of a compound. With the addition of hydrophobic organosilica moiety, TMMS considerably increased the hydrophobicity of the catalyst surface. Superhydrophobic film chemical sensors and hydrophobic polyester fabrics are successfully constructed by TMMS.³⁷ The present work revealed that the presence of methyl groups on the silica surface caused the decrease in surface hydrophilicity. The hydrophobicity of the $\text{ZrO}_2\text{-SiO}_2\text{-Me\&Et PhSO}_3\text{H}$ catalyst was also slightly improved with the incorporation of sulfonic acid groups.

3.1.5. Chemical Composition of Catalysts. **3.1.5.1. Fourier Transform Infrared (FT-IR) Spectroscopy.** The FT IR spectra of the $\text{ZrO}_2\text{-SiO}_2$ catalyst are shown in Figure 7, and they provide evidence for the formation of SiO_2 (red spectra). The significant bands at 1061 and 576 cm^{-1} are assigned to the Si–O–Si asymmetric stretching vibrations.^{19,27} Nonetheless, these bands did not appear in the spectra of blank ZrO_2 . The band at 1061 cm^{-1} was attributed to the asymmetric stretching vibrations, such as those of Si–O and Si–O–Zr. The bands

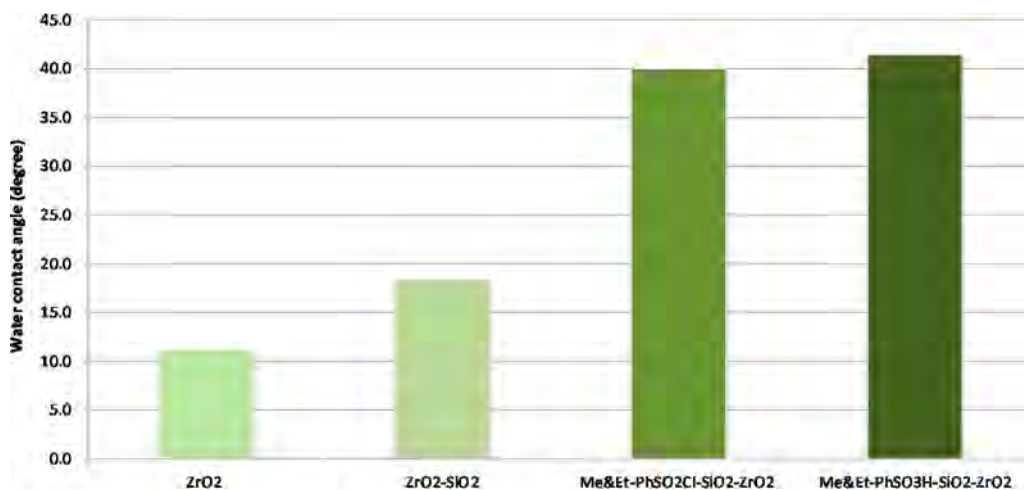


Figure 6. Hydrophobicity levels of ZrO_2 , $\text{ZrO}_2\text{-SiO}_2$, $\text{ZrO}_2\text{-SiO}_2\text{-Me\&Et PhSO}_2\text{Cl}$, and $\text{ZrO}_2\text{-SiO}_2\text{-Me\&Et PhSO}_3\text{H}$ based on water contact angle analysis.

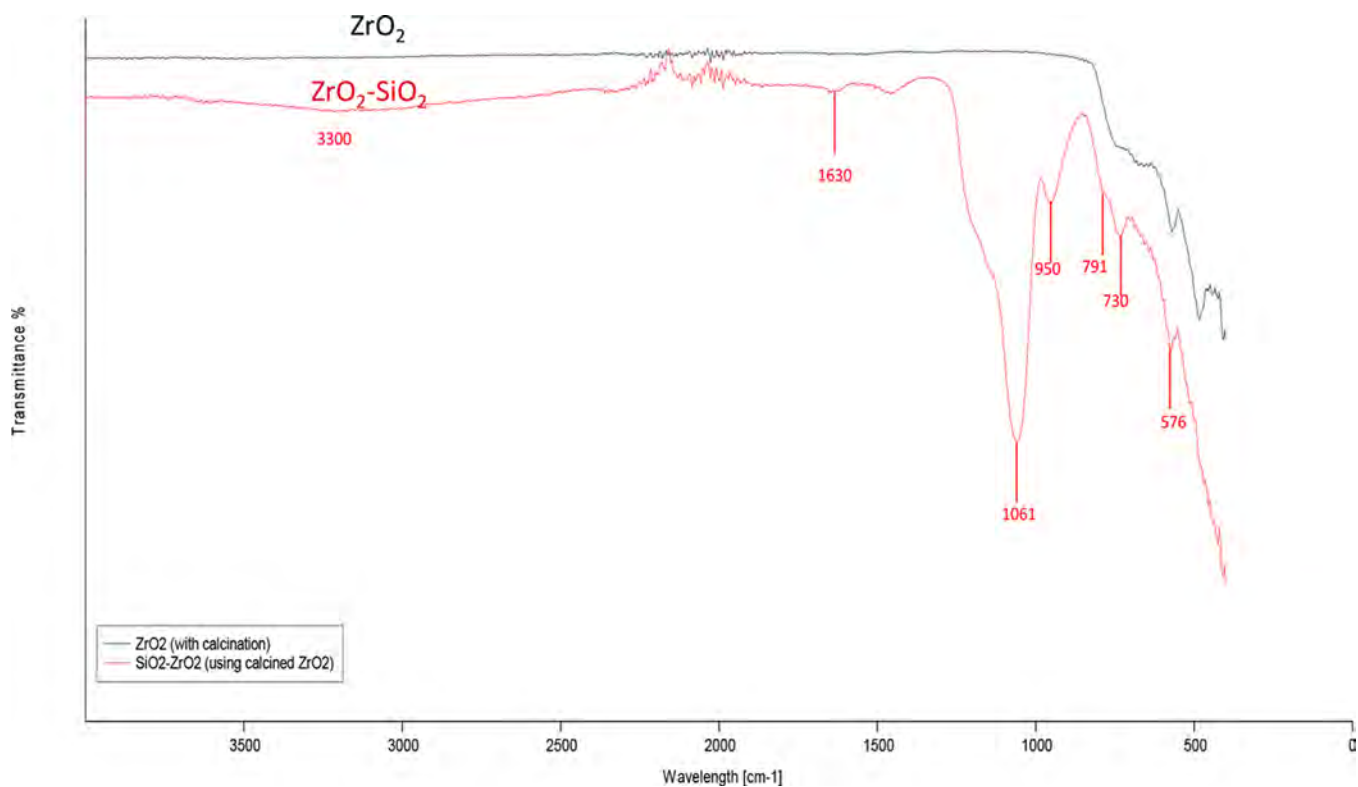


Figure 7. Fourier transform infrared spectra of ZrO₂-SiO₂ (black, ZrO₂; red, ZrO₂-SiO₂).

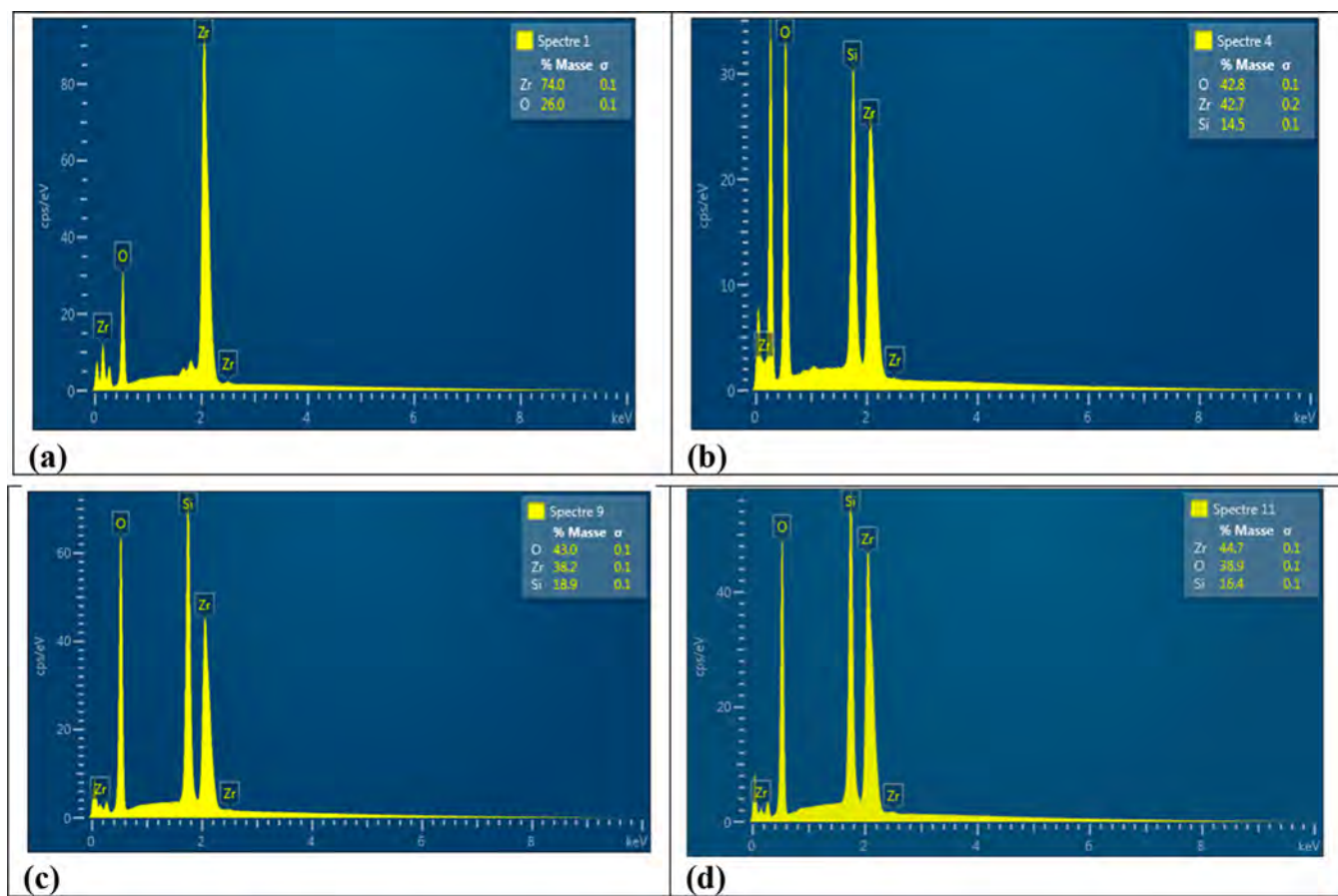


Figure 8. Energy dispersive X ray spectroscopy peaks of ZrO₂ (a), ZrO₂-SiO₂ (b), ZrO₂-SiO₂-Me&Et PhSO₃Cl (c), and ZrO₂-SiO₂-Me&Et PhSO₃H (d).

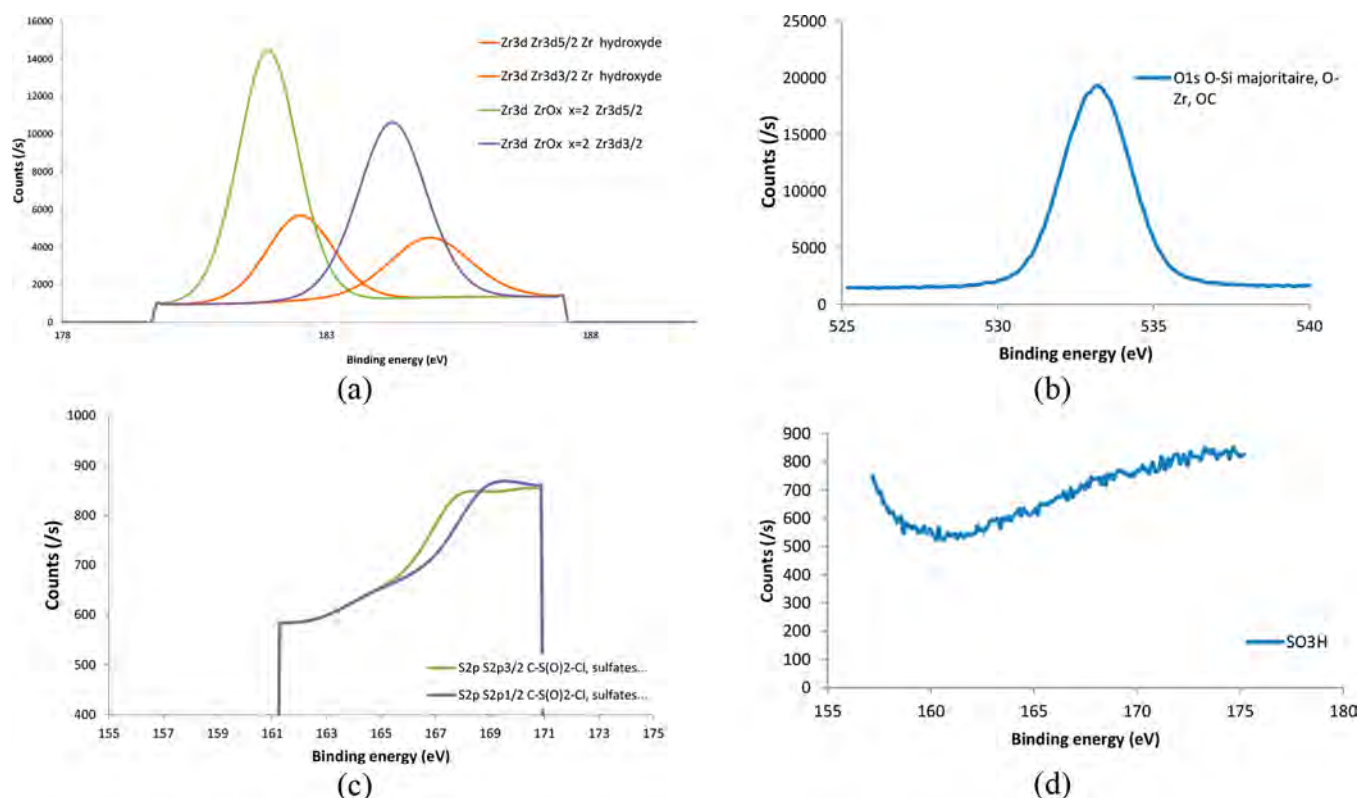
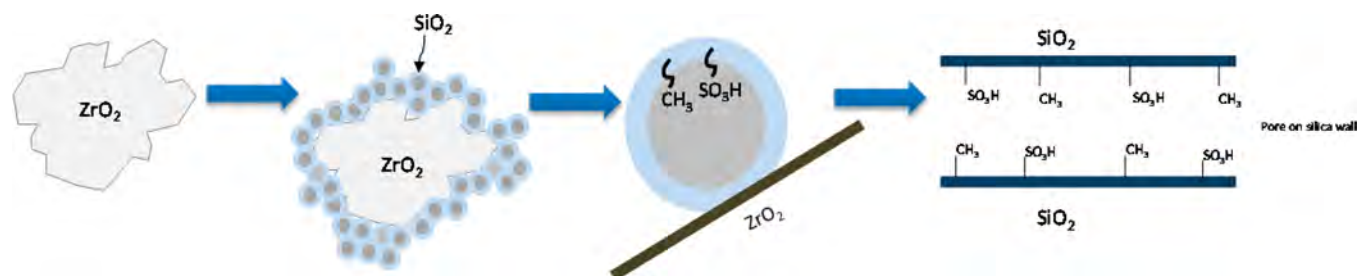


Figure 9. X ray photoelectron spectra for ZrO_2 (a), ZrO_2-SiO_2 (b), $ZrO_2-SiO_2-Me\&Et\ PhSO_2Cl$ (c), and $ZrO_2-SiO_2-Me\&Et\ PhSO_3H$ (d).

Scheme 1. Synthesis Diagram for the Surface Functionalization on the ZrO_2-SiO_2 Support



at approximately 791 and 730 cm^{-1} are associated with the formation of a condensed silica network.^{38,39} The band located around 950 cm^{-1} is given by the stretching vibrations of the Si-O bond.³⁸ The FT IR results confirmed the successful coating of SiO_2 .

3.1.5.2. Energy-Dispersive X-ray Spectroscopy (EDX) Analysis. EDX analysis was performed to identify the surface composition change in each modification step of the catalyst. As shown in Figure 8a, ZrO_2 support displayed Zr and O peaks, with averaged mass percentages of 74.2% Zr and 25.8% O. In ZrO_2-SiO_2 , the silica coated ZrO_2 consisted of an additional Si peak, as shown in Figure 8b. The averaged mass percentages of Zr, O, and Si are 42.7, 42.8, and 14.5%, respectively. The increase in the O compound was in agreement with the adherence of SiO_2 to the support.

The surface composition of $ZrO_2-SiO_2-Me\&Et\ PhSO_2Cl$ and $ZrO_2-SiO_2-Me\&Et\ PhSO_3H$ showed no significant change. The averaged surface composition of $ZrO_2-SiO_2-Me\&Et\ PhSO_2Cl$ comprised 39.77% Zr, 42.2% O, and 18.06% Si (Figure 8c). The Si content of $ZrO_2-SiO_2-Me\&Et\ PhSO_2Cl$ was 3.5% higher than that of ZrO_2-SiO_2 . The

discrepancy may be attributed to the ZrO_2-SiO_2 functionalized with TMMS and CSPETS. The $ZrO_2-SiO_2-Me\&Et\ PhSO_3H$ peaks with 44.7% Zr, 38.9% O, and 16.4% Si are presented in Figure 8d. The sulfonated surface of the $ZrO_2-SiO_2-Me\&Et\ PhSO_3H$ catalyst showed 1.66% less Si content than that of $ZrO_2-SiO_2-Me\&Et\ PhSO_2Cl$.

3.1.5.3. X-ray Photoelectron Spectroscopy (XPS). XPS allows further insight analysis on the catalyst's surface composition. The surface composition of each modified catalyst was investigated using XPS (Figure 9). The binding energy in the interval range of 178–188 eV (Figure 9a) indicated that the ZrO_2 material belonged to Zr-O (182 and 185 eV), Zr-Ox, or Zr-OH groups (181 and 184 eV). For ZrO_2-SiO_2 (Figure 9b), the large peak at 533.1 eV suggested a high majority ratio mixture of SiO_2 with two different environments: Si-O-Si (533 eV) and Si-O-Zr (531 eV).⁴⁰ Meanwhile, the peak ranging from 160 to 170 eV was assigned to C-SO₂-Cl (168–169 eV) and sulfate groups (168.5 eV) in Figure 9c. This result can be attributed to CSPETS and TMMS agents on $ZrO_2-SiO_2-Me\&Et\ PhSO_2Cl$. Nevertheless, for $ZrO_2-SiO_2-Me\&Et\ PhSO_3H$

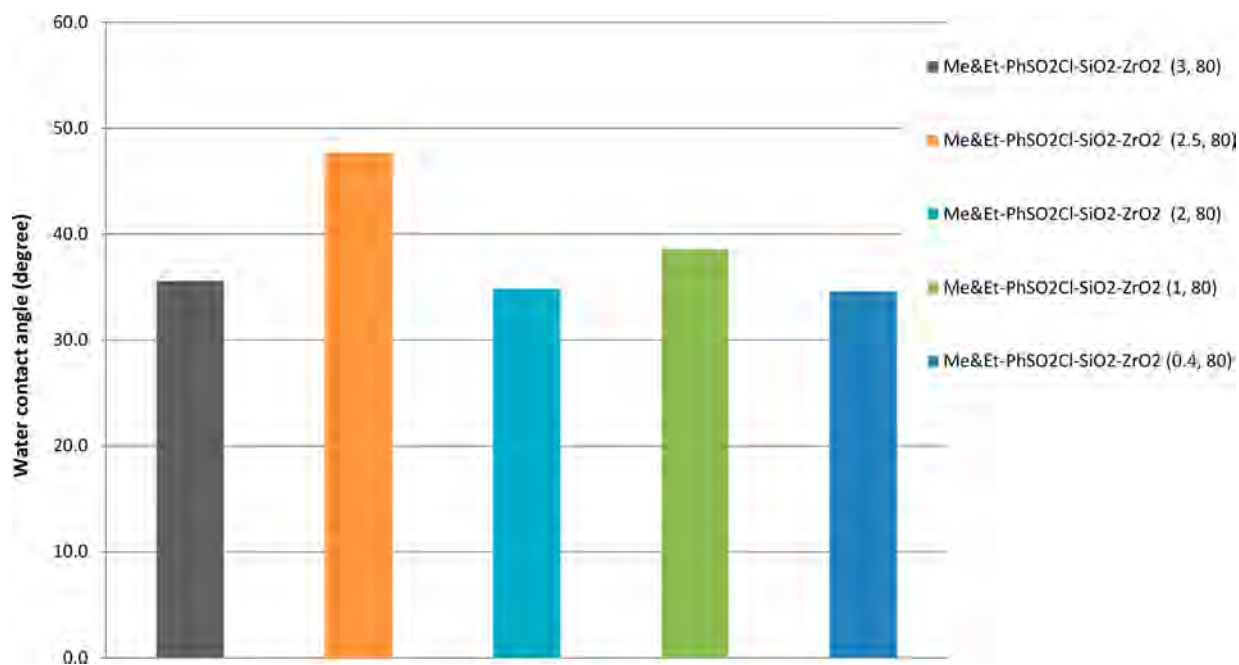


Figure 10. Effects of loading amount of TMMS–CSPETS on hydrophobicity levels of designed catalysts.

(Figure 9d), a limited percentage of the sulfonic group (silica composites of the SO₃H group) was detected at 168.5 eV in correspondence with the peak at 160–170 eV.³⁶ The obtained result may be attributed to the detection limit of XPS (about 10 nm) as it was inaccessible to a single monosphere particle with an approximate diameter of 400 nm. These results suggested that the sulfonic acid sites for the ZrO₂–SiO₂–Me&Et PhSO₃H catalyst were mainly distributed within the nanosphere pores of monosphere particle. This finding is similar to that of the previous work, which reported that most of the acidic sites for silica prepared catalysts are buried in the bulk polymer beads.¹⁹

3.1.6. Schematic of Catalyst Synthesis. Scheme 1 shows the schematic illustration for the synthesis of ZrO₂–SiO₂–Me&Et PhSO₃H catalyst. BET, FESEM, FT IR, EDX, and XPS results proved the successful coating of SiO₂ on ZrO₂ support. The strong adherence of SiO₂ to ZrO₂ support was mainly contributed by the OH[−] group of NH₄OH as the suspension of static repulsion against van der Waals attractive forces stabilizes the bonding of ZrO₂–SiO₂.³⁴ Moreover, the additional mass obtained in ZrO₂–SiO₂ confirmed the formation of SiO₂. The formation of covalent bonds on the ZrO₂–SiO₂ surface transformed the hydrophilic character to a hydrophobic one using the hydrophobic organosilica moiety TMMS was confirmed by contact angle analysis, BET, and XPS. This observation was also reported by Markovska et al.⁴¹ Hydrophobization involved the attachment of methyl groups from TMMS to a silicon atom; CSPETS was used to initiate the conversion of the silica surface to sulfonic moieties by exchanging Cl[−] with OH[−] during sulfonation. Sulfonic acid sites are considerably important for catalysis, as it was proven by commercial application of Amberlyst 15 in esterification²⁰ as well as production of solketal through acetalization of glycerol in the presence of sulfonic mesostructured silicas.⁴² The XPS and BET results suggested that SO₃H was mainly distributed in the mesopore of the nanospheres.

3.2. Control of the Hydrophobicity and Acidity of the Catalyst. This part investigated the effect of the loading

amount of TMMS–CSPETS on ZrO₂–SiO₂ support toward the hydrophobicity level of the catalyst. The total loading amount of both activation agents, which was expressed as the molar ratio of TMMS–CSPETS to ZrO₂–SiO₂, was optimized in the presence of a constant concentration of TMMS (80 mol %) to obtain the most suitable hydrophobicity level of the catalyst. Subsequently, the optimized ratio of CSPETS–TMMS to ZrO₂–SiO₂ was used to adjust the ratio of TMMS hydrophobic agent in mole percentage. Solid catalysts designed with different TMMS amounts, namely, ZrO₂–SiO₂–Me&Et PhSO₃H 50, ZrO₂–SiO₂–Me&Et PhSO₃H 70, and ZrO₂–SiO₂–Me&Et PhSO₃H 80, were produced and applied in catalytic activity screening.

3.2.1. Effects of Loading Amount of TMMS–CSPETS on Catalyst Hydrophobicity. The effects of the amount of functionalization agents (TMMS–CSPETS) must be investigated to obtain the highest possible hydrophobicity level of the designed catalyst. The molar ratio of activation agents to the ZrO₂–SiO₂ support was initially optimized at a constant concentration (80 mol %) of TMMS. Afterward, the suitable CSPETS:TMMS ratio was optimized to obtain the most suitable catalyst acidity and hydrophobicity. In this study, the loading weights of TMMS–CSPETS ranged from 0.2 to 1.2 g to functionalize 1 g of ZrO₂–SiO₂. The loading amounts of CSPETS and TMMS on ZrO₂–SiO₂ are presented in Table S1 (Supporting Information).

The effects of the loading amount of TMMS on the hydrophobicity level of the designed catalysts are illustrated in Figure 10. Results revealed that the 2.5:1 molar ratio of SiO₂ to TMMS–CSPETS (ZrO₂–SiO₂–Me&Et PhSO₂Cl (2.5, 80)) achieved the highest performance among the designed catalysts because it exhibited the highest hydrophobicity level. The experimental work also proved that the hydrophobicity level of the catalyst was unaltered by loading an excessive amount of total agents. For instance, the corresponding 1.6 g of CEPETS and 1.6 g of TMMS were loaded excessively to 1 g of SiO₂–ZrO₂ to gain a highly hydrophobic surface catalyst in designing the ZrO₂–SiO₂–Me&Et PhSO₂Cl (0.4, 80) catalyst, but the

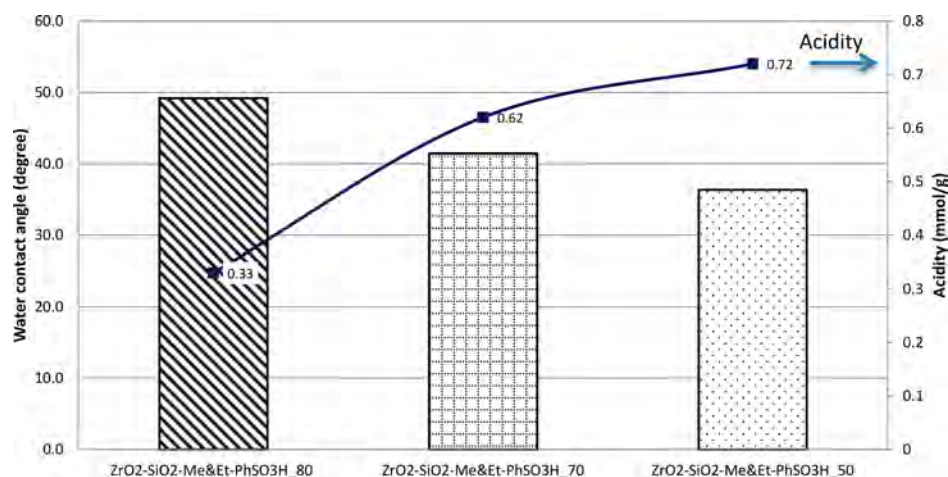


Figure 11. Relationship of hydrophobicity level and acidity of designed catalysts.

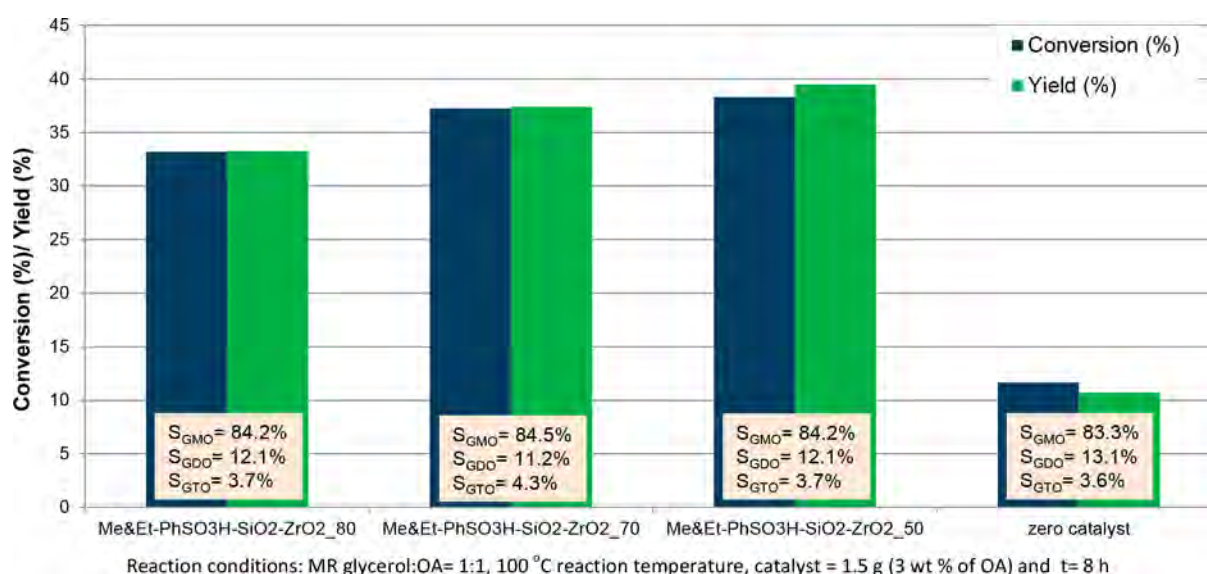


Figure 12. Performance evaluation of designed catalysts.

highest hydrophobicity was not achieved. This work evidenced that further increase in the loading amount of CSPETS and TMMS will not improve the catalyst hydrophobicity. Furthermore, no direct relation existed between the amount of CSPETS and TMMS loading and the hydrophobicity level. This study confirmed that the best molar ratio of SiO₂ to the total agents was 2.5:1, and the catalyst with the highest hydrophobicity was ZrO₂-SiO₂-Me&Et PhSO₂Cl (2.5, 80).

3.2.2. Effect of TMMS Loading on Catalyst Acidity. Section 3.2.1 identified 2.5:1 as the most suitable molar ratio of SiO₂ to the total agents. Different mole percentages of TMMS were used to investigate the hydrophobicity level of each designed catalyst at a constant molar ratio of SiO₂:TMMS-CSPETS (2.5:1). The mole percentages of TMMS utilized to adjust the hydrophobicity level of the designed catalysts, which were ZrO₂-SiO₂-Me&Et PhSO₃H 80, ZrO₂-SiO₂-Me&Et PhSO₃H 70, and ZrO₂-SiO₂-Me&Et PhSO₃H 50, are shown in Table S2 (Supporting Information). With consideration of the hydrophobicity and exchangeable capacity of CSPETS of the catalyst, this study used no TMMS ratio that is less than 50 mol % in preparing acid catalyst with good hydrophobicity at more than 40° in contact angle analysis.

Results confirmed that ZrO₂-SiO₂-Me&Et PhSO₃H 80 possessed a hydrophobicity level higher than those of ZrO₂-SiO₂-Me&Et PhSO₃H 70 and ZrO₂-SiO₂-Me&Et PhSO₃H 50, which reasonably agreed with the relative amount of TMMS (i.e., the highest TMMS amount was utilized for ZrO₂-SiO₂-Me&Et PhSO₃H 80) (Table S2). The experimental results also showed that the loading amount of TMMS affected the acidity of the designed catalyst. The relationship of the acidity and hydrophobicity of the designed catalysts is illustrated in Figure 11; increasing the catalyst hydrophobicity can decrease the catalyst acidity.

3.3. Effects of Hydrophobicity and Acidity of Designed Catalysts on Catalytic Activities. **3.3.1. Catalytic Activity: Influence on Conversion and Yield.** The designed catalysts with different hydrophobicity and acidity levels (ZrO₂-SiO₂-Me&EtPhSO₃H 80, ZrO₂-SiO₂-Me&Et PhSO₃H 70, and ZrO₂-SiO₂-Me&EtPhSO₃H 50) were used in comparative studies on glycerol esterification with OA. All the reactions were conducted at an equimolar OA to glycerol ratio, 100 °C reaction temperature, 3 wt % catalyst concentration with respect to the OA weight, and solventless reaction conditions for 8 h. Figure 12 shows the catalytic

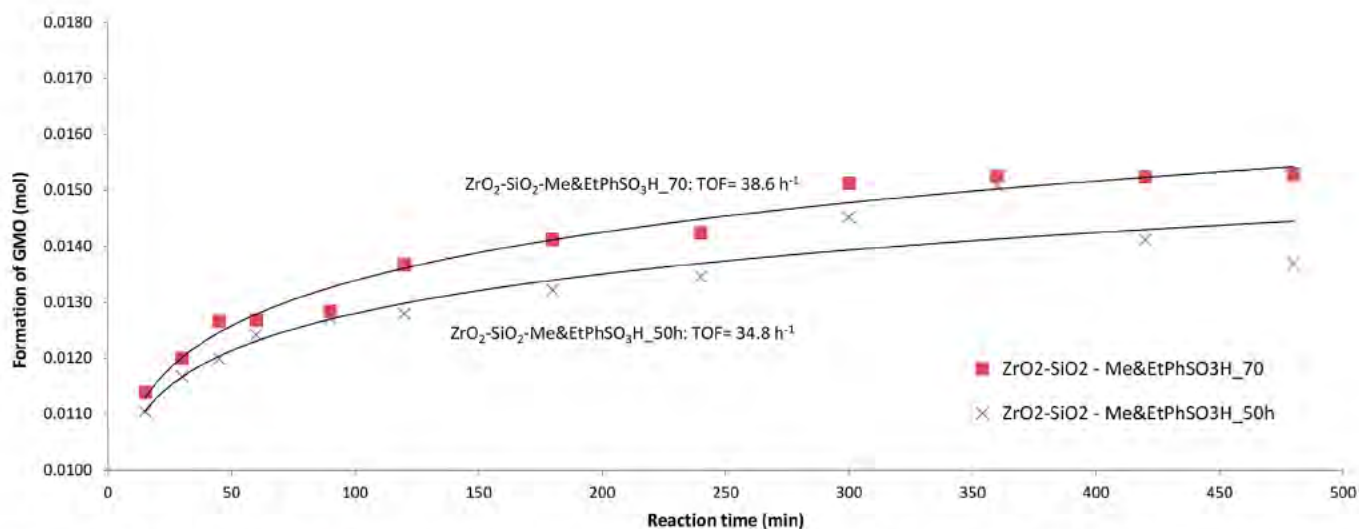
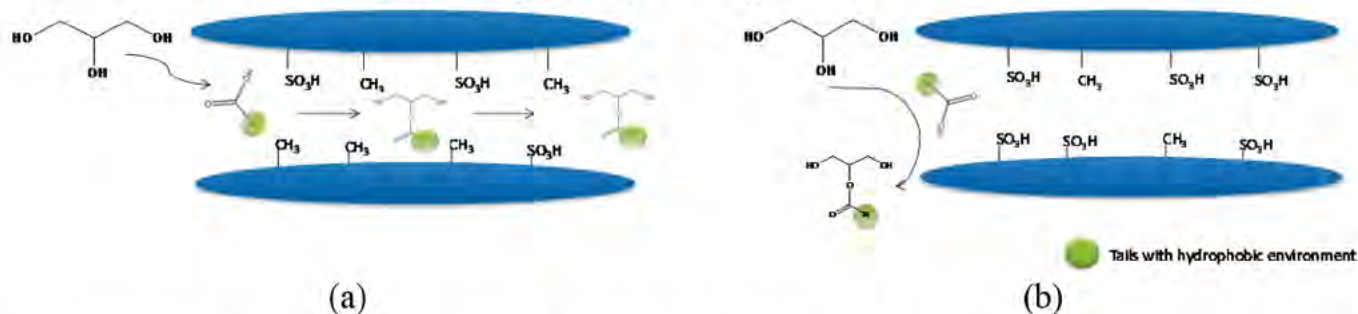


Figure 13. Effects of catalyst hydrophobicity on formation rate of GMO in the presence of $\text{ZrO}_2\text{-SiO}_2\text{-Me\&EtPhSO}_3\text{H}$ 70 and $\text{ZrO}_2\text{-SiO}_2\text{-Me\&EtPhSO}_3\text{H}$ 50h catalysts.

Scheme 2. Influence of Surface Hydrophobicity on Catalytic Activity^a



^a(a) Hydrophobic surface contains higher methyl groups within the mesoporous framework. (b) Hydrophobic surface contains lesser methyl groups within the mesoporous framework.

activities of the designed catalysts, which were also compared with the results in the absence of catalyst.

The obtained results demonstrated that the acidity of the catalyst significantly affected the conversion and yield. Results showed that catalytic activity increased with increased catalyst acidity, following the order $\text{ZrO}_2\text{-SiO}_2\text{-Me\&EtPhSO}_3\text{H}$ 50 (acidity, 0.72 mmol/g; yield, 39.5%) > $\text{ZrO}_2\text{-SiO}_2\text{-Me\&EtPhSO}_3\text{H}$ 70 (acidity, 0.62 mmol/g; yield, 37.4%) > $\text{ZrO}_2\text{-SiO}_2\text{-Me\&EtPhSO}_3\text{H}$ 80 (acidity, 0.33 mmol/g; yield, 33.3%). Nevertheless, the yield difference between $\text{ZrO}_2\text{-SiO}_2\text{-Me\&EtPhSO}_3\text{H}$ 50 and $\text{ZrO}_2\text{-SiO}_2\text{-Me\&EtPhSO}_3\text{H}$ 70 was only 2%. The results also indicated the selectivity obtained for these three designed catalysts are almost identical ($S_{\text{GMO}} = 84\%$ and $S_{\text{GDO}} = 12\%$), and this reasonably agreed with product selectivity was affected by pore structure of catalyst⁷ as the textural properties of $\text{ZrO}_2\text{-SiO}_2\text{-Me\&EtPhSO}_3\text{H}$ are similar despite their different hydrophobicity and acidity levels. This study suggested that $\text{ZrO}_2\text{-SiO}_2\text{-Me\&EtPhSO}_3\text{H}$ 70 catalyst is the best catalyst for this reaction with consideration of the following: (i) the amount of CSPETS used in catalyst synthesis (as the cost of CSPETS used to synthesize $\text{ZrO}_2\text{-SiO}_2\text{-Me\&EtPhSO}_3\text{H}$ 70 was 12% less than that of $\text{ZrO}_2\text{-SiO}_2\text{-Me\&EtPhSO}_3\text{H}$ 50); (ii) the insignificant difference (2%) in the yield obtained between $\text{ZrO}_2\text{-SiO}_2\text{-Me\&EtPhSO}_3\text{H}$ 50 and $\text{ZrO}_2\text{-SiO}_2\text{-Me\&EtPhSO}_3\text{H}$ 70.

3.3.2. Catalytic Activity: Role of Hydrophobicity in GMO Production. The role of hydrophobicity in the catalytic glycerol esterification with OA at a constant catalyst acidity level must be evaluated to eliminate the effect of catalyst acidity in this investigation. Hence, $\text{ZrO}_2\text{-SiO}_2\text{-Me\&EtPhSO}_3\text{H}$ 50h was synthesized by using a 50% lower amount of TMMS at constant CSPETS loading than that of the high performing $\text{ZrO}_2\text{-SiO}_2\text{-Me\&EtPhSO}_3\text{H}$ 70 catalyst (refer to Table S3, Supporting Information). $\text{ZrO}_2\text{-SiO}_2\text{-Me\&EtPhSO}_3\text{H}$ 50h and $\text{ZrO}_2\text{-SiO}_2\text{-Me\&EtPhSO}_3\text{H}$ 70 catalysts possessed identical acidity levels (0.62 mmol/g).

This comparative study demonstrated the role of the hydrophobicity of acid catalyst in increasing the reaction yield (37.4% vs 28.9%) at identical reaction conditions. Moreover, this study confirmed that the hydrophobicity of acid catalysts enhanced the formation rate of GMO, which is well illustrated in Figure 13. The plot revealed that the reaction rate of $\text{ZrO}_2\text{-SiO}_2\text{-Me\&EtPhSO}_3\text{H}$ 70 was faster (turnover frequency (TOF) = 38.6 h^{-1}) than that of $\text{ZrO}_2\text{-SiO}_2\text{-Me\&EtPhSO}_3\text{H}$ 50h (34.8 h^{-1}). The acidity of catalyst was constant in this study, and therefore good accessibility within mesoporous catalytic sites is the governing factor in obtaining better product yield. The presence of higher methyl groups (higher amount of TMMS hydrophobization agent utilized) within the mesoporous network of $\text{ZrO}_2\text{-SiO}_2\text{-Me\&EtPhSO}_3\text{H}$ 70 resulted in better diffusion of OA, and the

Table 2. Comparison of Catalytic Activity between ZrO₂-SiO₂-Me&EtPhSO₃H 70 and Several Other Catalysts Reported in the Literature^a

catalyst	reaction parameters			performance		ref
	temp (°C)	catal concn (wt %)	time (h)	conv (%)	selectivity (%)	
ZrO ₂ -SiO ₂ -Me&EtPhSO ₃ H ₇₀ acidity = 0.63 mmol/g	100	3	8	39	S _{GMO} = 84.5 S _{GDO} = 11.2 S _{GTO} = 4.3	this work
MCM-4-methyl-SO ₃ H acidity = 1.7 mmol/g	120	5	8	89	S _{GMO} = 40	43
HPW/Cu ₃ (BTC) ₂ ^b acidity = NA	120	1	8	45	S _{GMO} = 62	22
Fe-Zn DMC complex acidity = 1.06 mmol/g	180	8	8	63.4	S _{GMO} = 67.3 S _{GDO} = 31.7	21
Ti-SBA-16 acidity = 0.09 mmol/g	180	3	3	72.8	S _{GMO} = 32.8 S _{GDO} = 57.9 S _{GTO} = 9.2	25

^aAll the reactions were conducted at equimolar ratio of glycerol to OA, catalyst concentration was with respect to OA, and solventless conditions.

^bTin-organic framework.

catalytic reaction occurred within the silica pores. This result reasonably agreed with that reported by Jérôme et al.¹³ By contrast, ZrO₂-SiO₂-Me&EtPhSO₃H 50h with reduced methyl groups did not benefit from the mesoporous structure as catalysis can only take place at the pore entrance due to poor diffusion of OA within the silica pore structure, which resulted in lower catalyst activity. In brief, the results demonstrated that catalytic activity improved with the increase of hydrophobic methyl groups of the mesoporous framework. Scheme 2 illustrates the influence of surface hydrophobicity on catalytic activity.

A comparison of catalytic activity between ZrO₂-SiO₂-Me&EtPhSO₃H 70 and several other catalysts reported in the literature is summarized in Table 2. All the reactions were conducted at an equimolar glycerol to OA ratio. The conversion (40%) for ZrO₂-SiO₂-Me&EtPhSO₃H 70 catalyst at 100 °C reaction temperature was lower than that of the MCM 4 methyl SO₃H catalyst (89%) at 120 °C. This discrepancy was mainly attributed to the acidity (1.7 mmol/g) of the MCM 4 methyl SO₃H catalyst. However, the GMO selectivity for MCM 4 methyl SO₃H was 40%, which is 2 times lower than that of ZrO₂-SiO₂-Me&EtPhSO₃H 70. The catalyst developed in this work showed a better performance than that of the tin-organic framework (HPW/Cu₃(BTC)₂) catalyst with conversions of 45 and 62% GMO selectivity at 120 °C.

Nonetheless, the catalyst activity of ZrO₂-SiO₂-Me&EtPhSO₃H 70 (40% conversion) was considered remarkable compared with that of the Fe-Zn DMC complex subjected to a high reaction temperature (Table 2). The Fe-Zn DMC complex obtained conversions of 63.4 and 67.3% GMO selectivity despite being operated at a high reaction temperature (180 °C) and high loading catalyst concentration (8 wt %). The hydrophobicity enhanced titanium silicate type catalyst (Ti-SBA 16) achieved a conversion of 72.8% at 180 °C and short reaction time (3 h) and showed the potential of ZrO₂-SiO₂-Me&EtPhSO₃H 70 to perform well at a long reaction time.

3.3.3. Catalyst Stability Studies. The stability of the ZrO₂-SiO₂-Me&EtPhSO₃H 70 catalyst was studied by separating the reaction mixture after reaction. The recovered catalyst was directly applied in the subsequent reaction cycle without any further treatment. The catalyst recyclability experiments were

performed under the following optimized operating parameters: 160 °C, temperature; 5 wt % catalyst concentration; equimolar glycerol to OA ratio; 650 rpm stirring speed; 480 min reaction time. Catalyst recyclability and stability experiment revealed that the yield decreased with the number of uses in Figure 14. The yield was reduced from 83, 74, and 69% in

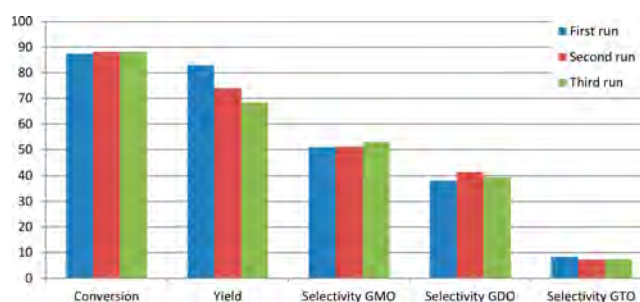


Figure 14. Catalyst stability study on ZrO₂-SiO₂-Me&EtPhSO₃H 70 catalyst at an equimolar glycerol to oleic acid ratio, 5 wt % catalyst concentration of OA, 160 °C reaction temperature, 650 rpm speed, and 480 min reaction time.

accordance with the number of times of usage. Herein, “yield” refers to the total GMO, GDO, and GTO in product mixtures, respectively. This trend may be attributed to that the GTO product blocks the active centers of the catalyst or the hydrophobic properties are lost.⁸ The contact angle analysis result of the spent catalyst was inferior (31.9°) to that of the newly developed catalyst with 41.5°; this indicated leaching possibilities of the functionalities attached on the surface of the catalysts. The decreased yield in Figure 14 also indicated the formation of potential side products, such as acrolein, polyglycerol, or polyglycerol esters.¹³ This result showed that the good hydrophobicity of a catalyst most probably minimized the undesirable side reaction.

4. CONCLUSIONS

A novel highly hydrophobic ZrO₂-SiO₂ based acid catalyst was successfully developed in this work. Mesoporous organo sulfonic acid functionalized heterogeneous catalyst can be developed by following proper silication on zirconia and functionalization steps. It can be concluded that the loading

amounts of TMMS and CSPETS are vital in controlling hydrophobicity and acidity of catalyst under similar catalyst preparation methods. Among the catalysts tested in this work, $ZrO_2-SiO_2-Me&Et\ PhSO_3H$ 70 catalyst with 70 mol % TMMS and 0.62 mmol/g acidity is the best catalyst for glycerol esterification with OA. It is shown that increases of hydrophobicity of catalyst can decrease the acidity of the designed catalyst. Nevertheless, this work evidenced that the hydrophobicity has significant influence on GMO yield and reaction rate. The yield of GMO was 3 times higher than zero catalyst reaction at equimolar oleic acid to glycerol ratio, 100 °C reaction temperature, and 3 wt % catalyst concentrations with respect to weight of OA for 8 h.

■ ASSOCIATED CONTENT

● Supporting Information

The Supporting Information is available free of charge on the ACS Publications website at DOI: 10.1021/acs.iecr.8b01609.

Loading amounts of TMMS and CSPETS in ZrO_2-SiO_2 support and in designing different acidities of catalysts; designed catalysts with different TMMS loading amounts (PDF)

■ AUTHOR INFORMATION

Corresponding Author

*Tel.: +6037491 8622, ext 7166. Fax: +6035635 8630. E mail: kheireddinea@sunway.edu.my.

ORCID

Mohamed Kheireddine Aroua: 0000 0002 9388 5439

Notes

The authors declare no competing financial interest.

■ ACKNOWLEDGMENTS

The authors would like to express gratitude to the financial support provided by INCREASE CNRS France and High Impact Research (HIR) Grant (UM.C/625/1/HIR/MOHE/ENG59). The dual Ph.D. scholarship (University of Malaya) and French government sponsorship (Embassy France, Malaysia) are gratefully acknowledged.

■ REFERENCES

- (1) Kong, P. S.; Aroua, M. K.; Daud, W. M. A. W. Conversion of crude and pure glycerol into derivatives: A feasibility evaluation. *Renewable Sustainable Energy Rev.* **2016**, *63*, 533–555.
- (2) Oleoline Oleoline Glycerine Market Report. http://www.hbint.com/datas/media/590204fd077a6e381ef1a252/sample_quarterly_glycerine.pdf.
- (3) Suprun, W.; Lutecki, M.; Haber, T.; Papp, H. Acidic catalysts for the dehydration of glycerol: Activity and deactivation. *J. Mol. Catal. A: Chem.* **2009**, *309* (1–2), 71–78.
- (4) Kong, P. S.; Aroua, M. K.; Daud, W. M. A. W.; Lee, H. V.; Cognet, P.; Peres, Y. Catalytic role of solid acid catalysts in glycerol acetylation for the production of bio additives: a review. *RSC Adv.* **2016**, *6* (73), 68885–68905.
- (5) Vol'eva, V. B.; Belostotskaya, I. S.; Malkova, A. V.; Komissarova, N. L.; Kurkovskaya, L. N.; Usachev, S. V.; Makarov, G. G. New approach to the synthesis of 1,3 dioxolanes. *Russ. J. Org. Chem.* **2012**, *48* (5), 638–641.
- (6) Singh, D.; Patidar, P.; Ganesh, A.; Mahajani, S. Esterification of Oleic Acid with Glycerol in the Presence of Supported Zinc Oxide as Catalyst. *Ind. Eng. Chem. Res.* **2013**, *52* (42), 14776–14786.
- (7) Konwar, L. J.; Mäki Arvela, P.; Kumar, N.; Mikkola, J. P.; Sarma, A. K.; Deka, D. Selective esterification of fatty acids with glycerol to monoglycerides over –SO₃H functionalized carbon catalysts. *React. Kinet., Mech. Catal.* **2016**, *119* (1), 121–138.
- (8) Zhang, Z.; Huang, H.; Ma, X.; Li, G.; Wang, Y.; Sun, G.; Teng, Y.; Yan, R.; Zhang, N.; Li, A. Production of diacylglycerols by esterification of oleic acid with glycerol catalyzed by diatomite loaded SO₄²⁻/TiO₂. *J. Ind. Eng. Chem.* **2017**, *53*, 307–316.
- (9) Kao Corporation GRAS STATUS OF DAG. <https://www.fda.gov/downloads/food/ingredientspackaginglabeling/gras/noticeinventory/ucm266329.pdf>.
- (10) Kong, P. S.; Aroua, M. K.; Daud, W. M. A. W. Catalytic esterification of bioglycerol to value added products. *Rev. Chem. Eng.* **2015**, *31* (5), 437–451.
- (11) Kuwahara, Y.; Kaburagi, W.; Nemoto, K.; Fujitani, T. Esterification of levulinic acid with ethanol over sulfated Si doped ZrO₂ solid acid catalyst: Study of the structure–activity relationships. *Appl. Catal., A* **2014**, *476*, 186–196.
- (12) Dabbawala, A. A.; Mishra, D. K.; Huber, G. W.; Hwang, J. S. Role of acid sites and selectivity correlation in solvent free liquid phase dehydration of sorbitol to isosorbide. *Appl. Catal., A* **2015**, *492*, 252–261.
- (13) Jérôme, F.; Pouilloux, Y.; Barrault, J. Rational Design of Solid Catalysts for the Selective Use of Glycerol as a Natural Organic Building Block. *ChemSusChem* **2008**, *1* (7), 586–613.
- (14) Narkhede, N.; Patel, A. Sustainable valorisation of glycerol via acetalization as well as carboxylation reactions over silicotungstates anchored to zeolite H β . *Appl. Catal., A* **2016**, *515*, 154–163.
- (15) Gonçalves, M.; Rodrigues, R.; Galhardo, T. S.; Carvalho, W. A. Highly selective acetalization of glycerol with acetone to solketal over acidic carbon based catalysts from biodiesel waste. *Fuel* **2016**, *181*, 46–54.
- (16) Gaudin, P.; Jacquot, R.; Marion, P.; Pouilloux, Y.; Jérôme, F. Acid Catalyzed Etherification of Glycerol with Long Alkyl Chain Alcohols. *ChemSusChem* **2011**, *4* (6), 719–722.
- (17) Estevez, R.; López, M. I.; Jiménez Sanchidrián, C.; Luna, D.; Romero Salguero, F. J.; Bautista, F. M. Etherification of glycerol with tert butyl alcohol over sulfonated hybrid silicas. *Appl. Catal., A* **2016**, *526*, 155–163.
- (18) Kong, P. S.; Aroua, M. K.; Daud, W. M. A. W.; Cognet, P.; Peres, Y. Enhanced microwave catalytic esterification of industrial grade glycerol over Brønsted based methane sulfonic acid in production of biolubricant. *Process Saf. Environ. Prot.* **2016**, *104*, 323–333.
- (19) Chen, J.; Chen, J.; Zhang, X.; Gao, J.; Yang, Q. Efficient and stable PS SO₃H/SiO₂ hollow nanospheres with tunable surface properties for acid catalyzed reactions. *Appl. Catal., A* **2016**, *516*, 1–8.
- (20) Åkerman, C. O.; Gaber, Y.; Ghani, N. A.; Lämsä, M.; Hatti Kaul, R. Clean synthesis of biolubricants for low temperature applications using heterogeneous catalysts. *J. Mol. Catal. B: Enzym.* **2011**, *72* (3), 263–269.
- (21) Kotwal, M.; Deshpande, S. S.; Srinivas, D. Esterification of fatty acids with glycerol over Fe–Zn double metal cyanide catalyst. *Catal. Commun.* **2011**, *12* (14), 1302–1306.
- (22) Wee, L. H.; Lescouet, T.; Fritsch, J.; Bonino, F.; Rose, M.; Sui, Z.; Garrier, E.; Packet, D.; Bordiga, S.; Kaskel, S.; Herskowitz, M.; Farrusseng, D.; Martens, J. A. Synthesis of Monoglycerides by Esterification of Oleic Acid with Glycerol in Heterogeneous Catalytic Process Using Tin–Organic Framework Catalyst. *Catal. Lett.* **2013**, *143* (4), 356–363.
- (23) Hamerski, F.; Prado, M. A.; da Silva, V. R.; Voll, F. A. P.; Corazza, M. L. Kinetics of layered double hydroxide catalyzed esterification of fatty acids with glycerol. *React. Kinet., Mech. Catal.* **2016**, *117* (1), 253–268.
- (24) Hamerski, F.; Corazza, M. L. LDH catalyzed esterification of lauric acid with glycerol in solvent free system. *Appl. Catal., A* **2014**, *475* (0), 242–248.
- (25) Kotwal, M.; Kumar, A.; Darbha, S. Three dimensional, mesoporous titanosilicates as catalysts for producing biodiesel and biolubricants. *J. Mol. Catal. A: Chem.* **2013**, *377*, 65–73.

- (26) Isahak, W. N. R. W.; Ramli, Z. A. C.; Ismail, M.; Yarmo, M. A. Highly Selective Glycerol Esterification over Silicotungstic Acid Nanoparticles on Ionic Liquid Catalyst. *Ind. Eng. Chem. Res.* **2014**, *53* (25), 10285–10293.
- (27) Saravanan, K.; Tyagi, B.; Bajaj, H. C. Esterification of stearic acid with methanol over mesoporous ordered sulfated ZrO₂-SiO₂ mixed oxide aerogel catalyst. *J. Porous Mater.* **2016**, *23*, 937–946.
- (28) Hirakawa, T.; Tanaka, S.; Usuki, N.; Kanzaki, H.; Kishimoto, M.; Kitamura, M. A Magnetically Separable Heterogeneous Dealylation Catalyst: [CpRu(η^3 -C₃H₅)(2-pyridinecarboxylato)]PF₆ Complex Supported on a Ferromagnetic Microsize Particle Fe₃O₄@SiO₂. *Eur. J. Org. Chem.* **2009**, *2009* (6), 789–792.
- (29) Mobaraki, A.; Movassagh, B.; Karimi, B. Hydrophobicity enhanced magnetic solid sulfonic acid: A simple approach to improve the mass transfer of reaction partners on the surface of the heterogeneous catalyst in water generating reactions. *Appl. Catal., A* **2014**, *472*, 123–133.
- (30) Lee, K. W. Y.; Porter, C. J. H.; Boyd, B. J. A Simple Quantitative Approach for the Determination of Long and Medium Chain Lipids in Bio relevant Matrices by High Performance Liquid Chromatography with Refractive Index Detection. *AAPS PharmSci Tech* **2013**, *14*, 927–934.
- (31) Thommes, M.; Kaneko, K.; Neimark, A. V.; Olivier, J. P.; Rodríguez Reinoso, F.; Rouquerol, J.; Sing, K. S. W. Physisorption of gases, with special reference to the evaluation of surface area and pore size distribution (IUPAC Technical Report). *Pure Appl. Chem.* **2015**, *87*, 1051–1069.
- (32) Zhao, H.; Chen, J.; Sun, Y. Effect Of Calcination Temperature on the Performance of Co/ZrO₂ Catalysts for Fischer–Tropsch Synthesis. *Prepr. Pap. Am. Chem. Soc., Div. Fuel Chem.* **2003**, *48* (2), 733.
- (33) Rahman, I. A.; Padavettan, V. Synthesis of Silica Nanoparticles by Sol Gel: Size Dependent Properties, Surface Modification, and Applications in Silica Polymer Nanocomposites A Review. *J. Nano mater.* **2012**, *2012*, 132424.
- (34) Wang, X. D.; Shen, Z. X.; Sang, T.; Cheng, X. B.; Li, M. F.; Chen, L. Y.; Wang, Z. S. Preparation of spherical silica particles by Stöber process with high concentration of tetra ethyl orthosilicate. *J. Colloid Interface Sci.* **2010**, *341* (1), 23–29.
- (35) Bazula, P. A.; Arnal, P. M.; Galeano, C.; Zibrowius, B.; Schmidt, W.; Schüth, F. Highly microporous monodisperse silica spheres synthesized by the Stöber process. *Microporous Mesoporous Mater.* **2014**, *200*, 317–325.
- (36) Fang, W.; Wang, S.; Liebens, A.; De Campo, F.; Xu, H.; Shen, W.; Pera Titus, M.; Clacens, J. M. Silica immobilized Aquivion PFSA superacid: application to heterogeneous direct etherification of glycerol with n butanol. *Catal. Sci. Technol.* **2015**, *5* (8), 3980–3990.
- (37) Li, L.; Li, B.; Dong, J.; Zhang, J. Roles of silanes and silicones in forming superhydrophobic and superoleophobic materials. *J. Mater. Chem. A* **2016**, *4* (36), 13677–13725.
- (38) Faria, E. A.; Marques, J. S.; Dias, I. M.; Andrade, R. D. A.; Suarez, P. A. Z.; Prado, A. G. S. Nanosized and reusable SiO₂/ZrO₂ catalyst for highly efficient biodiesel production by soybean transesterification. *J. Braz. Chem. Soc.* **2009**, *20*, 1732–1737.
- (39) Wang, P.; Liu, H.; Niu, J.; Li, R.; Ma, J. Entangled Pd complexes over Fe₃O₄@SiO₂ as supported catalysts for hydrogenation and Suzuki reactions. *Catal. Sci. Technol.* **2014**, *4* (5), 1333–1339.
- (40) Rodríguez Castellón, E.; Jiménez López, A.; Maireles Torres, P.; Jones, D. J.; Rozière, J.; Trombetta, M.; Busca, G.; Lenarda, M.; Storaro, L. Textural and structural properties and surface acidity characterization of mesoporous silica zirconia molecular sieves. *J. Solid State Chem.* **2003**, *175* (2), 159–169.
- (41) Markovska, I.; Yovkova, F.; Minov, G.; Rusev, D.; Lyubchev, L. Investigation of Silane Modified Ceramic Surface of Porous Mullite Ceramics. *Int. J. Environ. Ecol. Eng.* **2013**, *7* (7), 409.
- (42) Vicente, G.; Melero, J. A.; Morales, G.; Paniagua, M.; Martín, E. Acetalisation of bio glycerol with acetone to produce solketal over sulfonic mesostructured silicas. *Green Chem.* **2010**, *12* (5), 899–907.
- (43) Díaz, I.; Mohino, F.; Pérez Pariente, J. n.; Sastre, E. Synthesis of MCM 41 materials functionalised with dialkylsilane groups and their catalytic activity in the esterification of glycerol with fatty acids. *Appl. Catal., A* **2003**, *242* (1), 161–169.